Design and Microfabrication of an Electrostatically Actuated Scanning Micromirror with Elevated Electrodes

Mohd Haris*, Hongwei Qu*, Ankur Jain** and Huikai Xie**

*Department of Electrical and Computer Engineering, Oakland University, Rochester, Michigan 48309, USA
**Department of Electrical and Computer Engineering, University of Florida, Gainesville, Florida 32611, USA

ABSTRACT

This paper reports the design and microfabrication of an electrostatically actuated CMOS-MEMS micromirror with elevated electrodes. Two sets of bimorphs are employed to create mismatched vertical comb drives for mirror actuation. Device structural design and fabrication process are detailed and device performance such as scanning angles is simulated using CoventorWare, an integrated MEMS simulator. With a 26 V driving voltage applied to the mismatched comb drives alternately, a rotational angle of over ±12° can be realized. The device chips were fabricated using AMI 0.5 µm CMOS technology through MOSIS. DRIE post-CMOS microfabrication was performed for device release.

Keywords: CMOS-MEMS, electrostatic, micromirror, vertical comb-drive

1 INTRODUCTION

Electrostatic actuation has advantages of easy implementation and low actuation power. Vertical comb drives (VCD) have been studied for sensing and driving of a wide variety of optical and other MEMS devices [1-4]. Micromirrors using VCDs have demonstrated fast scanning speed and low actuation power. Some research groups have reported a 1-Dimensional VCD micromirrors with optical scan angles of 25° at 34 kHz [1] and 40° at 5.8 kHz [2], while other group has reported a 2D VCD micromirror that can scan optical angles greater than 15° in both *x* and *y* directions [3]. Vertical displacement of 7.5 µm [4] and even as high as 55 µm [5] have been achieved through the use of electrostatic VCDs. Angled VCDs have been reported that scanned optical angles greater than ±9° at 18 Vdc [6], and ±3° at 100 Vdc [7]. The driving voltage required by these devices ranges from as low as 10V [5] to as high as 250 V [1].

Existing VCD manufacturing processes are complicated and expensive. Most MEMS VCDs are currently fabricated using non-CMOS compatible processing methods, such as multiple wafer bonding and SOI processing [1-5]. This paper presents a novel design methodology for the fabrication of VCDs using foundry-CMOS compatible processes. This mask-less CMOS-compatible process has the potential to make VCD enabled devices and device arrays less expensive through batch fabrication.

2 DEVICE DESIGN

Figure 1 shows a 3D model of the designed device. Two sets of complementarily-oriented bimorphs elevate the stator electrodes above the corresponding rotor electrodes that are anchored to substrate through a pair of compliant torsional springs [8]. The inset in Fig. 1 shows part of the VCDs formed by the stators and rotors. The uniqueness of this structure also includes the integration of polysilicon heaters in the bimorph beams, as shown in Fig. 2. By passing current in these polysilicon heaters, the bimorph beams, which consist of SiO_2 and aluminum thin films, can be electrothermally driven to tune the elevation height of the stator comb fingers for maximum electrostatic actuation.

To allow rotational motion of the mirror plate, the bimorph sets elevating the stator electrodes are designed stiffer than the torsional mechanical springs connecting the mirror plate to the silicon substrate. A resonant frequency ratio of over 4 was chosen between the bimorph beams and

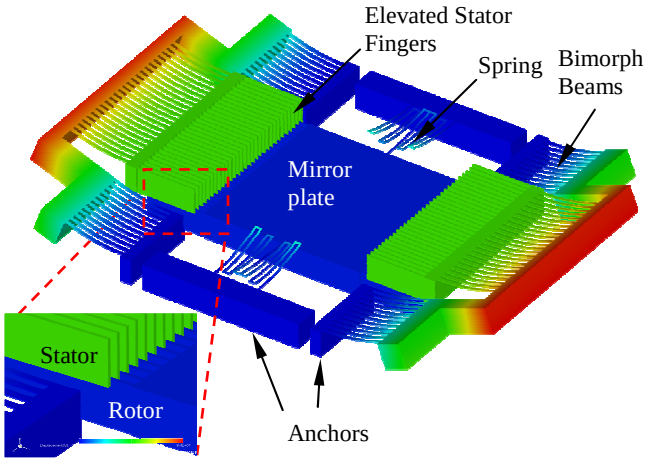

Figure 1. 3D model of the device with inset showing the VCD formed by elevated stator comb fingers and stator comb fingers on mirror plate.

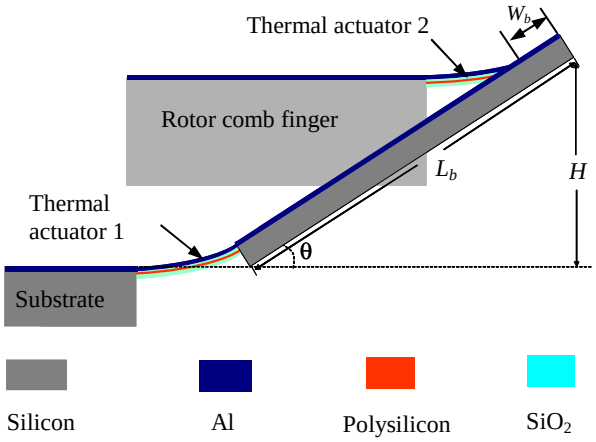

Figure 2. Bimorphs with embedded polysilicon actuators.

torsional springs to ensure stable operation of the device. Major parameters of the device are shown in Table 1.

Table 1: Major parameters of the device.

Parameter	Definition	Value
Mirror Length	l_m	0.4 mm
Mirror Width	w_m	0.4 mm
SCS Thickness	t	60 μm
VCD Finger Gap	g	2 μm
VCD Finger Width	w_f	6 μm
VCD Finger Length	l_f	100 μm
Number of Fingers	N_f	25
Length of bimorph beam	l_b	150 μm
Width of bimorph beam	w	9 μm
Width of connecting beam	w_b	50 μm
Thickness of beam	t	1.8 μm
Number of bimorph beams in LVD	N	24

The two sets of bimorph beams are used as a large-vertical-displacement (LVD) microactuator [9]. They are complementarily oriented in a folded rigid beam such that the curling of the two sets of bimorph beams compensates each other. This unique configuration results in a pure vertical elevation of the attached comb fingers once the comb drives are released from the substrate, as shown in Fig. 2. The elevation, H of the stator comb finger can be determined as

$$H = (L_b - W_b)\sin\theta \quad (1)$$

where, W_b is the width of the rigid beam connecting the two bimorph sets, and θ is the tilt angle of the amplifier beam. The vertical bending and the resultant torsional stiffness of the LVD bimorph beams can be calculated from [6] by

$$k_{Z\_LVD} = N\frac{Ewt^3}{4l_b^3} \quad (2)$$

$$k_{\phi\_LVD} = k_{z\_LVD}(l_b + \frac{L_b}{2})^2 \quad (3)$$

The required torsional stiffness of the spring connecting the mirror plate to the substrate can be calculated using

$$k_\phi = M\frac{w_m^2}{12}w_R^2 \quad (4)$$

where M is mass of the mirror plate. For the device, the torsional spring constant is calculated to be k_ϕ = 1.2 x 10^{-8} Nm/rad for the desired resonance frequency of 1 kHz. The required length of the standard torsion bar can be determined using Eq. 5 [7]. In order to reduce the length of the spring, folded serpentine spring is used.

$$l_s = \frac{2Gw_s^3t_s}{3k_\phi}\left[1 - \frac{192}{\pi^5}\frac{w_s}{t_s}tanh(\frac{\pi t_s}{2w_s})\right] \quad (5)$$

where G is the shear modulus; t_s and w_s are the thickness and width of the spring, respectively.

When a voltage is applied between the rotor and stator comb fingers, the movable rotor fingers rotate about the torsion axis until the restoring torque generated by the spring balances the electrostatic torque. The electrostatic torque is given by

$$\tau_{VCD} = N_f\frac{\varepsilon_0}{g}\frac{\partial A}{\partial\theta}V^2 \quad (6)$$

The term corresponds to the increase in finger overlap area with changing angular rotation is shown in Fig. 3 and is given by

$$\frac{\partial A}{\partial\theta} = \frac{1}{2}\left[\left(l_f + \frac{l_m}{2}\right)^2 - \left(\frac{1}{2}l_m\right)^2\right] \quad (7)$$

Balancing the electrostatic torque equation with the restoring torque equation of the spring, we get

$$\theta(V) = \frac{N_f\varepsilon_0}{2k_\phi g}V^2\left[l^2 - \left(\frac{l_m}{2}\right)^2\right] \quad (8)$$

The maximum rotation angle of the micromirror can be expressed by [7]

$$\theta_{\max} = \frac{t}{l_f + \frac{l_m}{2}} = 12^o \quad (9)$$

The corresponding rotation angle versus the applied

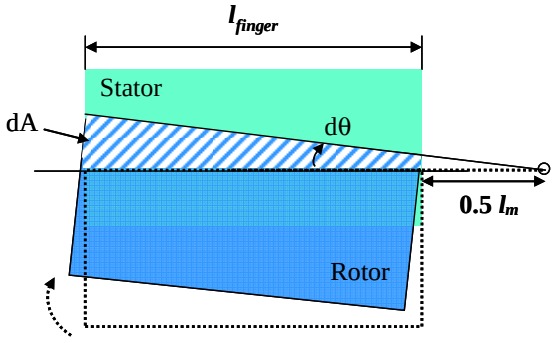

Figure 3. Cross-section of VCD for mirror rotation analysis.

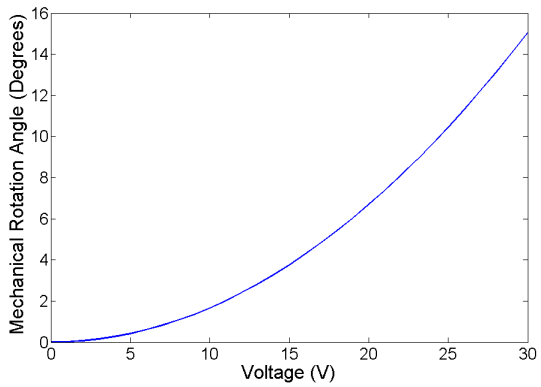

Figure 4. Mirror voltage versus applied dc voltage.

voltage plot as obtained using Eq. (8) is shown in Fig. 4. From Fig. 4, it is predicted that the mirror rotates ±12° at 26 V. In order to generate vertical motion, the two sets of electrostatic comb drives (on either end of the mirror plate) should be excited simultaneously. When the same voltage is simultaneously supplied to both VCD sets, the lower rotor fingers displace vertically upward due to the vertical electrostatic force as shown in Fig. 5.

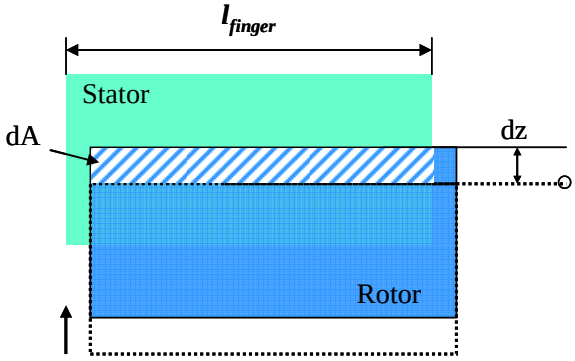

Figure 5. VCD analysis for mirror piston motion

This electrostatic force, generated by one pair of the VCD fingers is given by

$$F = \frac{1}{2} \cdot \frac{dC_z}{dz} \cdot V^2 \qquad (10)$$

where ε_0 is the dielectric constant of air between the comb drive, and V is the voltage applied to the comb drive. A factor of $2N_f$ should be applied to this electrostatic force since there are a total of $2N_f$ pairs of comb fingers that contribute towards the vertical actuation.

Fig. 6 shows the relation between the capacitance, and electrostatic force between the rotor and stator when applied a dc voltage from 0.001 V to 32 V.

3 FABRICATION PROCESS

AMI 0.5µm technology with three metal layers was used for the LVD mirror design and fabrication. Because of the

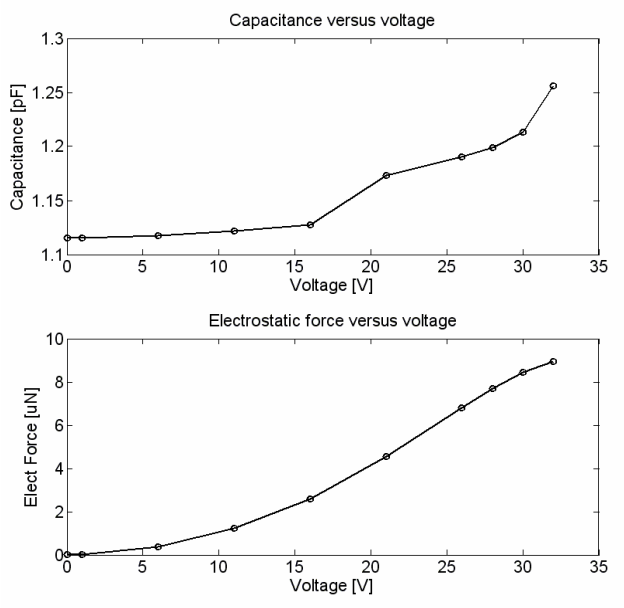

Figure 6. Simulation results of change of the VCD capacitance, electrostatic force versus applied voltage.

difference in the width of LVD bimorph and VCD finger, these two structures cannot be released at the same time. Two release steps were designed and performed to form the bimorphs and VCD fingers separately. When bimorphs are etched and undercut, top metal layer M3 was used as the mask to protect other structures. The device fabrication process flow is illustrated in Fig. 7. It is a maskless post-CMOS micromachining process in which top metal layers were used as etching mask in the dry etch processes [10].

The post-CMOS process starts with the backside etching to define the mirror plate thickness of 50µm. (Fig. 7(a)). Then anisotropic SiO_2 etching is performed to expose the regions for bimorph beams (Fig. 7(b)). A unique wet aluminum (Al) etching is followed to remove the top Al layer M3 (Fig. 7(c)). Next, a deep silicon etch followed by an isotropic silicon etch is performed to undercut the silicon

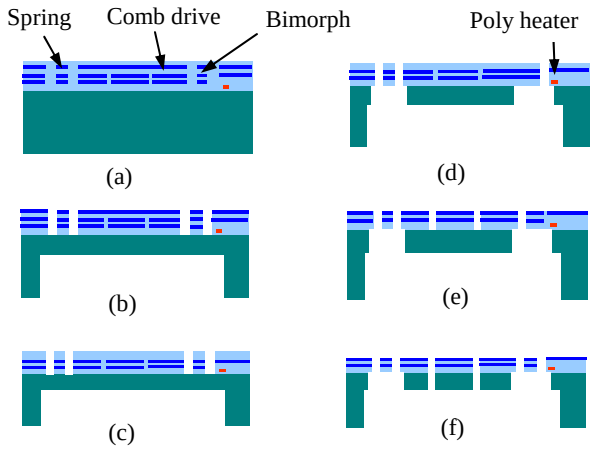

Figure 7. Microfabrication process flow.

underneath the bimorph beams and mirror springs (Fig. 7(d)). This step also electrically isolates the comb fingers on mirror plates and LVD plate from silicon substrate. Next, the second anisotropic SiO_2 etch defines VCD comb fingers (Fig. 7(e)). Finally, a deep silicon etch is performed again to etch through the comb fingers (Fig. 7(f)).

4 FABRICATION RESULTS

Fig. 8 shows the SEM image of the fabricated device. After the release process, the stators of the LVD on both sides were elevated above the substrate with a horizontal surface, validating the effective compensation of the two bimorph sets. Due to the larger tensile stress in the SiO_2 layer in the bimorphs beams, the elevation of VCD was measured as approximately 100 μm from the substrate. The resistance of the functional polysilicon heater was measured as 2.3 kΩ. Because of the fabrication variations caused by the timing-controlled etch, the single crystal silicon under the stator LVD was measured as 40 μm. Due to the large residual stress caused by the foundry CMOS process, and the abrupt release in the plasma etching chamber where high vacuum was present, the mirror plate broke at the connections to torsional springs. The bimorph actuator remained functional. A new microfabrication process is under development to avoid the sudden release of the device in high vacuum chamber that causes the structure damage.

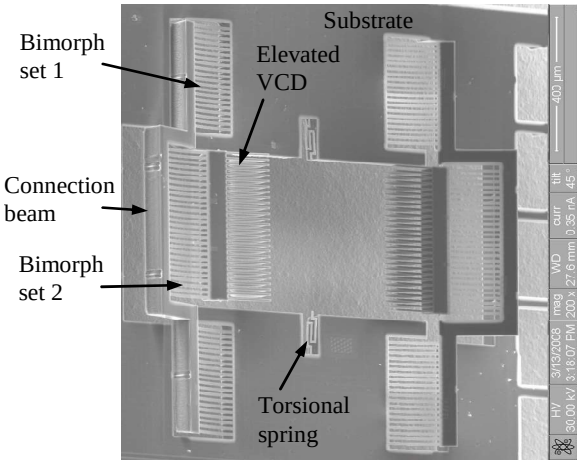

Figure 8. SEM image of the fabricated device.

5 CONCLUSION

An electrostatic micromirror capable of rotational and vertical piston motion has been designed and fabricated. The novel LVD structure elevates the stator fingers 100 μm above the substrate plane. This elevation can be tuned by passing current through the polysilicon actuator embedded in the bimorphs. This mirror can provide bi-directional scanning angles of ±12° at less than 30 V dc.

Maskless post-CMOS process was employed in the device fabrication. Since this mask-less fabrication process is foundry-CMOS compatible, it has the potential to be cost effective over other existing complex processes that are currently used in fabricating VCDs. The bi-directional rotational scanning and vertical piston motion scanning capabilities of this device make it useful in the areas of optical coherence tomography (OCT), adaptive optics and interferometry systems.

ACKNOWLEDGEMENTS

The device microfabrication was performed at the Michigan Nanofabrication Facility (MNF), one of sites in the NSF supported NNIN network. The authors would also like to thank Kai Sun at the Electron Microbeam Analysis Laboratory at the University of Michigan for assistance in SEM imaging of the device.

REFERENCES

1. R. A. Conant, et al., *Technical Digest of the 2000 Solid-State Sensor & Actuator Workshop*, Hilton Head, SC, pp.6-9.
2. U. Krishnamoorthy, et al., *J. of Microelectromechanical Systems*, **12**, pp. 458 – 464 (2003).
3. S. Kwon, et al., *IEEE Journal of Selected Topics in Quantum Electronics*, **10**, pp.498-504 (2004).
4. D. Lee, et al., *Technical Digest of Transducer'03*, pp. 576-579.
5. S. Kwon, etc al., *Technical Digest of the 2002 Solid-State Sensor & Actuator Workshop*, Hilton Head, SC, June 2002, pp.227-230.
6. H. Xie, etc al., *Journal of Microelectromechanical Systems*, **12**, pp. 450 - 457.
7. P. Patterson, etc al., *The Fifteenth IEEE International Conference on Micro Electro Mechanical Systems*, MEMS 2002, pp. 544-547.
8. A. Jain, etc al., *Sensor & Actuators A*, **122**, pp. 9-15 (2005).
9. A. Jain, etc al., *Technical Digest of 2004 Solid State Sensor, Actuator and Microsystems Workshop*, Hilton Head, SC, June 2004, pp. 228-231.
10. H. Xie, L. Erdmann, X. Zhu, K. Gabriel and G.K. Fedder, *J. of Microelectromechanical Systems* **11**, pp. 93-101 (2002).